Published OnlineFirst January 28, 2021; DOI: 10.1158/0008-5472.CAN-20-1822

3D Functional Genomics Screens Identify CREBBP as a Targetable Driver in Aggressive Triple-Negative Breast Cancer

Barrie Peck[1,2], Philip Bland[1,2], Ioanna Mavrommati[1,2], Gareth Muirhead[1], Hannah Cottom[1,2], Patty T. Wai[1,2], Sarah L. Maguire[1,3], Holly E. Barker[1,4], Eamonn Morrison[1], Divya Kriplani[1], Lu Yu[5], Amy Gibson[1,2], Giulia Falgari[1,2], Keith Brennan[6], Gillian Farnie[7], Richard Buus[1], Rebecca Marlow[1,8], Daniela Novo[1], Eleanor Knight[1], Naomi Guppy[1], Daniela Kolarevic[9], Snezana Susnjar[10], Natasa Medic Milijic[11], Kalnisha Naidoo[1], Patrycja Gazinska[1], Ioannis Roxanis[1], Sunil Pancholi[1], Lesley-Ann Martin[1], Erle M. Holgersen[1], Maggie C.U. Cheang[12], Farzana Noor[1], Sophie Postel-Vinay[13,14], Gerard Quinn[3], Simon McDade[3], Lukas Krasny[2], Paul Huang[2], Frances Daley[1], Fredrik Wallberg[1], Jyoti S. Choudhary[5], Syed Haider[1], Andrew N. Tutt[1,8], and Rachael Natrajan[1,2]

ABSTRACT

Triple-negative breast cancers (TNBC) are resistant to standard-of-care chemotherapy and lack known targetable driver gene alterations. Identification of novel drivers could aid the discovery of new treatment strategies for this hard-to-treat patient population, yet studies using high-throughput and accurate models to define the functions of driver genes in TNBC to date have been limited. Here, we employed unbiased functional genomics screening of the 200 most frequently mutated genes in breast cancer, using spheroid cultures to model *in vivo*–like conditions, and identified the histone acetyltransferase CREBBP as a novel tumor suppressor in TNBC. CREBBP protein expression in patient tumor samples was absent in 8% of TNBCs and at a high frequency in other tumors, including squamous lung cancer, where CREBBP-inactivating mutations are common. In TNBC, CREBBP alterations were associated with higher genomic heterogeneity and poorer patient survival and resulted in upregulation and dependency on a FOXM1 proliferative program. Targeting FOXM1-driven proliferation indirectly with clinical CDK4/6 inhibitors (CDK4/6i) selectively impaired growth in spheroids, cell line xenografts, and patient-derived models from multiple tumor types with CREBBP mutations or loss of protein expression. In conclusion, we have identified CREBBP as a novel driver in aggressive TNBC and identified an associated genetic vulnerability in tumor cells with alterations in CREBBP and provide a preclinical rationale for assessing CREBBP alterations as a biomarker of CDK4/6i response in a new patient population.

Significance: This study demonstrates that CREBBP genomic alterations drive aggressive TNBC, lung cancer, and lymphomas and may be selectively treated with clinical CDK4/6 inhibitors.

Introduction

The genetic landscape of human cancers has been comprehensively mapped by large sequencing efforts such as The Cancer Genome Atlas (TCGA; refs. 1–3), which have revealed many of the recurrent mutation events that are present in different tumor types. However, most of these mutations have not as yet been established as *bona fide* "drivers" or exploited therapeutically. It remains a formidable challenge to investigate the "long tail" of driver mutations in relevant cancer models, however, the identification of novel cancer genes and resultant cancer-specific vulnerabilities is needed, in particular for aggressive tumor types that are resistant to current treatment options.

It is now appreciated that more complex models of cancer are required to fully appreciate the contributing factors that drive tumorigenesis *in vivo* and increase the efficacy of novel therapies that make the transition from preclinical models to clinical trials. One

[1]The Breast Cancer Now Toby Robins Research Centre, The Institute of Cancer Research, London, England, United Kingdom. [2]Division of Molecular Pathology, The Institute of Cancer Research, London, England, United Kingdom. [3]Centre for Cancer Research and Cell Biology, Queen's University Belfast, Belfast, Northern Ireland, United Kingdom. [4]Division of Stem Cells and Cancer, The Walter and Eliza Hall Institute of Medical Research, Melbourne, Victoria, Australia. [5]Division of Cancer Biology, The Institute of Cancer Research, London, England, United Kingdom. [6]Faculty of Life Sciences, University of Manchester, Manchester, England, United Kingdom. [7]SGC Oxford, University of Oxford, Oxford, England, United Kingdom. [8]Breast Cancer Now Research Unit, King's College London, London, England, United Kingdom. [9]The Royal Marsden NHS Foundation Trust, London, England, United Kingdom. [10]Department of Medical Oncology, The Institute of Oncology and Radiology of Serbia, Belgrade, Serbia. [11]Department of Pathology and Cytology, The Institute of Oncology and Radiology of Serbia, Belgrade, Serbia. [12]Clinical Trials and Statistics Unit, The Institute of Cancer Research, London, England, United Kingdom. [13]Department of Drug Development (DITEP), Gustave Roussy Cancer Campus, Université Paris-Saclay, Villejuif, France. [14]UMR981, ATIP-Avenir team, INSERM, Villejuif, France.

Note: Supplementary data for this article are available at Cancer Research Online (http://cancerres.aacrjournals.org/).

Current address for B. Peck: Translational Cancer Metabolism Team, Centre for Tumour Biology, Barts Cancer Institute, Cancer Research UK Centre of Excellence, Queen Mary University of London, Charterhouse Square, London, EC1 6BQ, United Kingdom.

P. Bland, I. Mavrommati, and G. Muirhead contributed equally to this article.

Corresponding Author: Rachael Natrajan, The Institute of Cancer Research, 237 Fulham Road, London, England, SW3 6JB, United Kingdom. Phone: 207-153-5546; Fax: 207-153-5340; E-mail: rachael.natrajan@icr.ac.uk

Cancer Res 2021;81:847–59

doi: 10.1158/0008-5472.CAN-20-1822

Published OnlineFirst January 28, 2021; DOI: 10.1158/0008-5472.CAN-20-1822

high-throughput way of achieving this is through the use of 3D spheroid cultures, which more accurately recapitulate the *in vivo* features of cancer, such as hypoxia, altered cell–cell contacts, and metabolism (4, 5), and allow high-throughput assessment of novel genetic dependencies involved in cancer progression.

Current therapeutic strategies for the treatment of human cancers using precision medicine approaches have achieved clinical success through either direct targeting of oncogenic dependencies (e.g., HER2-targeted therapy in HER2-amplified breast cancer), or through synthetic lethal approaches (e.g., the use of PARP inhibitors in BRCA1/2-mutant ovarian and breast cancers; refs. 6, 7). Synthetic lethality is an attractive strategy for many cancer-associated genomic alterations; however, it is reliant on distinct genetic alterations in cancer cells that can act as predictive biomarkers to enable upfront patient stratification. Identification of additional patient populations who would benefit from treatment with clinically approved therapies would fast track these indications through clinical trials. This is a desirable strategy in particular for the most aggressive subtype of breast cancer, triple-negative breast cancer (TNBC), which lacks expression of estrogen receptor (ER), progesterone receptor, or HER2 receptors. TNBCs are heterogeneous with a significant number of patients having a high risk of early metastatic relapse, which are commonly resistant to standard-of-care chemotherapy treatments (8, 9). TNBCs show a distinct repertoire of copy-number alterations, mutations, and mRNA expression, compared with hormone receptor–positive tumors, and are characterized with higher levels of genomic instability (1, 2). TNBCs display a high frequency of mutations in *TP53*, while they also display a significant burden of mutations in a myriad of other genes, albeit at a lower frequency (1). However, despite progress in characterizing the genomic landscape of TNBCs, the majority of these mutations have not been established as "drivers," that is, have not been functionally tested, meaning targetable biological dependencies remain elusive (10). Together, this highlights the urgent need to identify molecular drivers of TNBC disease progression to identify actionable alterations that would increase the therapeutic options for these patients.

In this study we aimed to (i) establish the functional impact of recurrently mutated genes in TNBC, (ii) identify how to target these through synthetic lethal approaches, and (iii) assess whether these findings could be extended to other hard-to-treat aggressive cancers. Using a functional genomics approach under conditions more similar to those encountered in the unfavorable tumor microenvironment, multicellular spheroid cultures, we silenced the 200 most frequently mutated genes in breast cancer, and identified that inactivation of the histone acetyltransferase (HAT) CREBBP significantly increased cell growth in cancer cells that experienced nutrient stress, such as hypoxia. We report that *CREBBP* protein expression is reduced in around one-fifth of TNBCs, and is associated with a poorer survival. CREBBP protein expression was also reduced in multiple other solid tumors, including bladder, endometrial, and squamous lung cancers, which harbor high frequencies of CREBBP mutations. We identified and validated a mechanism whereby loss of CREBBP activity results in the upregulation of and dependency on a FOXM1-driven transcriptional proliferative program that renders cells selectively sensitive to CDK4/6 inhibition. This is seen in multiple tumor types with CREBBP alterations, which we validated using both *in vitro* and *in vivo* models. On the basis of these data, we highlight that CREBBP loss plays an important role in driving the aggressive behavior of TNBC and other tumor types and propose that CREBBP should be assessed as a biomarker of CDK4/6 inhibitor (CDK4/6i) sensitivity in clinical trials, particularly in those tumor types where CREBBP genomic alterations are seen at high frequency.

Materials and Methods

Reagents and cell lines

The MCF10a cell line was purchased from the ATCC (RRID:CVCL_0598). The MCF10DCIS.com cell line was purchased from Asterand, Inc. (RRID:CVCL_5552). MCF10NeoT, MCF10AT1, MCF10Ca1a, MCF10Ca1d, and MCF10Ca1h (RRID:CVCL_5555, RRID:CVCL_6675, RRID:CVCL_6683, RRID:CVCL_5554, RRID:CVCL_6681, and RRID:CVCL_6679) were kindly provided by The Barbara Ann Karmanos Cancer Institute (Detroit, MI). All progression series cell lines were grown as described previously (11). Wild-type (WT) and CREBBP-mutant (CREBBPmut; HZGHC001109c005) cell lines were purchased from Horizon Discovery, and grown in Iscove's modified Dulbecco's media supplemented with 10% FBS and penicillin–streptomycin. DV-90, EVSA-T, SU-DHL-6, and NU-DHL-1 cell lines (RRID:CVCL_1184, RRID:CVCL_1207, RRID:CVCL_2206, and RRID:CVCL_1876) were purchased from DSMZ (Germany) and grown in RPMI media supplemented with 10% FBS and penicillin–streptomycin. AN3CA, NCI-H520, NALM-6, A549, H1299, HCT116, BT20, CAL-51, HCC70, HCC1937, HCC1806, Hs578t, and MDA-MB-157 cell lines (RRID:CVCL_0028, RRID:CVCL_1566, RRID:CVCL_0023, RRID:CVCL_0060, RRID:CVCL_0291, RRID:CVCL_0178, RRID:CVCL_1110, RRID:CVCL_1270, RRID:CVCL_0290, RRID:CVCL_1258, and RRID:CVCL_0332 RRID:CVCL_0618) were obtained from the ATCC and grown in RPMI media supplemented with 10% FBS and penicillin–streptomycin. All cell lines were grown in a humidified incubator at 37°C with 5% CO_2. Cell lines were periodically tested to confirm no *Mycoplasma* infection using MycoAlertTM Mycoplasma Detection Kit as per the manufacturer's instructions (Lonza). Cells were authenticated by short tandem repeat typing with the Geneprint10 Kit (Promega). Cells were kept for a maximum of 10–15 passages from time of thawing to experimentation.

siRNA spheroid screen

The gene library for the siRNA screen was chosen from a meta-analysis of published breast cancer sequencing studies (1, 12–16), choosing the top 200 recurrently mutated genes that encompassed the top 100 genes in ER^+, $HER2^+$, and TNBC, respectively (Supplementary Table S1). Reverse transfection siRNA spheroid screens were performed in triplicate as described previously (5, 11). MCF10a, MCF10NeoT, MCF10AT1, MCF10DCIS.com, MCF10Ca1a, MCF10Ca1d, and MCF10Ca1h cell lines were reverse transfected with 37.5 nmol/L of Dharmacon siGENOME siRNA using Lullaby Reagent (OZ Biosciences). BT20, CAL-51, HCC70, HCC1937, HCC1806, Hs578t, and MDA-MB-157 cell lines were reverse transfected with 37.5 nmol/L of Dharmacon siGENOME siRNA using Viromer (Lipocalyx GmbH). Cell viability was measured after 5 days by CellTiter-Glo. The progression series screen was analyzed using z-score analysis. The TNBC cell line–targeted screen was analyzed by plate median normalized values. Spheroids were imaged using a Nikon TE 2000 Inverted Wide-field Microscope fitted with a motorized stage, filter wheels, a Pro-Scan Controller (Prior Scientific), Shutter (Sutter Instruments), Orca R2 Camera (Hamamatsu), and 84000v2 DAPI/FITC/TRITC/Cy5 Quad (Chroma Technology). The microscope was operated by HCI imaging software 4.3.1.33. Experiments were carried out at 37°C (Solent Scientific) and 10% CO_2.

Published OnlineFirst January 28, 2021; DOI: 10.1158/0008-5472.CAN-20-1822

Short hairpin RNA cell line generation

To generate of doxycycline-inducible TetOnPLKO-shRNA cell lines, short hairpin RNA (shRNA) sequences targeting CREBBP or nontargeting control (NTC) were cloned into the TetOn-pLKO-puro lentiviral vector as described previously (17). Clone IDs for shRNAs are as follows: *shCREBBP* #27 (TRCN0000011027) and *shCREBBP* #81 (TRCN0000356081). Lentiviruses were produced by cotransfecting HEK293T cells with lentiviral and packaging plasmids pCMVΔR8.91 and pMD.G. Supernatants were collected 72 hours after transfection, mixed with polybrene (8 μg/mL), and used to infect cells. Cells were selected in medium containing puromycin (2 μg/mL).

Tissue microarrays

Tissue microarray (TMA) slides [BR10011a ($n = 100$), BL802a ($n = 60$), EMC1021 ($n = 97$), HLug-Squ150CS-01 ($n = 75$), and OV2084a ($n = 193$)] were purchased from US Biomax, Inc. An additional TNBC series "Belgrade" was assembled from a consecutive series of primary untreated cases ($n = 175$) from The Institute of Oncology and Radiology of Serbia (Belgrade, Serbia), with three representative cores per tumor. Written informed consent was obtained, where appropriate, from the patients, and studies were conducted in accordance with recognized ethical guidelines (Declaration of Helsinki and CIOMS) and were approved by an institutional review board. Antibody staining was performed (see Supplementary Methods). TMAs were assessed for nuclear CREBBP protein expression in the malignant epithelium only, using a modified Allred score. Only technically sound cores containing >20% invasive tumor cells were included in the analysis. Cores were evaluated by consultant pathologists (H. Cottom and I. Roxanis) for both intensity (0, no stain; 1, mild; 2, moderate; and 3, strong) and percentage of epithelial cells that stained positive (0, absent; 1, background; 2, 1%–25%; 3, 26%–50%; 4, 51%–75%; and 5, >75%; **Fig. 1**). Scores were derived from a sum of the intensity and percentage of immunoreactive cells; an average score of 0 for each tumor was considered as negative/absent, a score of 7 or 8 as high, a score of 4–6 as intermediate expression, and a score of <4 as low expression.

In vivo assessment of palbociclib efficacy

All animal work was carried out with UK Home Office approval. A total of 1×10^6 NCI-H520 cells or 2×10^6 SU-DHL-6 cells were injected subcutaneously with Matrigel into right flank of 8-week-old female NOD scid gamma (NSG) nude mice. Once tumors showed an increase in tumor size (caliper measurement), animals were randomized into two groups, which were treated orally with 100 mg/kg of palbociclib (Pfizer) or vehicle control (sodium lactate), daily. Operators were blinded to which cohort received palbociclib and to which cohort received vehicle. Tumor burden was calculated using the following equation: $v = 0.52 \times \text{length} \times \text{width}^2$ (the length should be recorded as the longest diameter). Animals were sacrificed when the humane endpoint was reached (12 mm in diameter). Statistical analysis was performed using Prism. *In vivo* efficacy for CTG-0869 and CTG-2055 was performed by Champions Oncology, where cells were implanted into 8-week-old female *nu/nu* nude mice. A surrogate of animal survival was determined when the tumor size reached a predefined volume of 500 mm^3 (SU-DHL-6 and NCI-H520) or 1,000 mm^3 (CTG-0869). Survival curves were analyzed by Kaplan–Meier method, with a log-rank Mantel–Cox test $P < 0.05$ being considered significant. Tumors were formalin-fixed and paraffin-embedded, and slides were stained with hematoxylin and eosin (H&E), or IHC was performed with antibodies against Ki-67 as described above.

Data availability

Raw proteomic data are available in PRIDE (RRID:SCR_012052) with accession no., PXD0120978. Single-cell data have been deposited in the European Nucelotide Archive with accession no., PRJEB32846. Code used in the analysis of this data is provided at https://zenodo.org/record/4020438.

Supplementary Materials and Methods online contain references (18–30).

Results

Identification of CREBBP as a novel driver in TNBC

To establish which recurrently mutated genes in TNBC operate as "drivers," we established an siRNA library that targeted the most frequently mutated genes ($n = 199$) in unselected breast cancers (**Fig. 1A**; Supplementary Table S1). We performed unbiased functional genomics screens with a two-pronged approach; using the isogenic MCF10 model of TNBC progression (MCF10 cell line progression series) and validation screen in a nonisogenic panel of TNBC cell lines, grown as 3D spheroids to recapitulate *in vivo*–like conditions, such as hypoxia and nutrient depletion (**Fig. 1B**; Supplementary Table S2; refs. 4, 5, 11, 31, 32). We chose the MCF10 progression series for an initial screen as we have shown previously that this is a good model to identify novel genetic dependencies involved in the progression of breast cancer when cells are grown in 3D, and although this model harbors an activating HRAS mutation, these have recently been found to be present in aggressive breast cancers (5, 11, 33). Analysis of the initial screen identified distinct known oncogenic dependencies, including *PIK3CA*, where reduced cell viability was seen only in cells harboring the H1047R hotspot mutation and a potential novel oncogenic dependency in cells harboring a SZT2 T211R mutation (Supplementary Fig. S1A). siRNAs targeting the known tumor suppressor genes *RB1* and *PTEN* caused a significant increase in viability in one or more cell lines, as well as a series of genes not previously implicated in TNBC, including *KMT2C, NIPBL*, and *CREBBP* (**Fig. 1B**; Supplementary Fig. S1B), suggesting loss of these genes may affect multiple stages of TNBC progression. Although we observed differences in the effect of gene silencing with some of these, perhaps due to genetic or epigenetic differences, the observed phenotypic effect in multiple cell lines, however, suggested these are *bona fide* driver genes. The majority of these effects were specific to 3D culture conditions (**Fig. 1C**; Supplementary Table S3), including *KMT2C, NIPBL*, and *CREBBP*, which promoted growth in multiple cell line spheroids, whereas silencing of *PTEN* had a smaller relative effect. To ascertain which alterations could be driving growth in diverse genetic backgrounds, we assessed the top 50 target gene siRNAs in a heterogeneous panel of TNBC cell line spheroids. This showed that silencing the lysine acetyltransferase *CREBBP* and *RB1* had the greatest impact on increasing viability across multiple TNBC cell lines (**Fig. 1D**; Supplementary Fig. S1C). In contrast to our findings in a 3D culture setting, assessment of CREBBP silencing from multiple large-scale publicly available 2D CRISPR and shRNA screens, did not result in an observed increased cellular viability when CREBBP was silenced (Supplementary Fig. S1D–S1F). Together, these results validate the primary screen in the MCF10 cells and show that CREBBP silencing also promotes growth in a 3D-specific manner in cancer cells derived from patients with TNBC. Interestingly, those cell lines that showed a significant growth advantage upon CREBBP silencing harbored an enrichment of *PIK3CA/PTEN* genomic alterations ($P = 0.0476$, Fisher exact test).

We next validated this finding using a number of orthogonal approaches. Deconvolution of siRNAs targeting *CREBBP* showed that

Published OnlineFirst January 28, 2021; DOI: 10.1158/0008-5472.CAN-20-1822

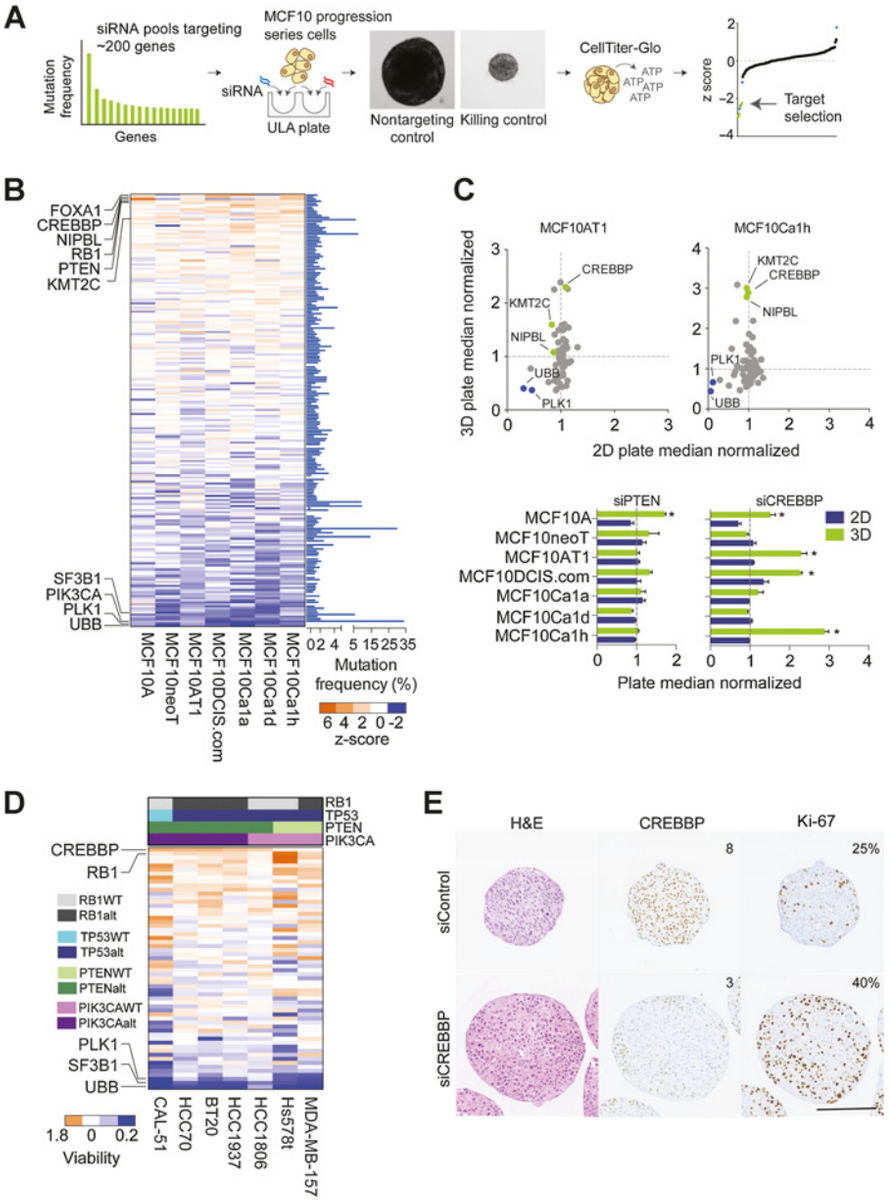

Figure 1.

A targeted functional genomics screen in cancer cell line spheroids identifies CREBBP as a tumor suppressor in TNBC. **A,** Schematic of reverse transfection protocol of spheroids in ultralow attachment plates. **B,** Heatmap of the z scores of the MCF10 progression series screen silencing the most frequently mutated genes (n = 199) in multicellular spheroids (3D cultures). Known killing controls (essential genes are highlighted: *SF3B1, PLK1, UBB*). **C,** Scatter plot of the spheroid viability of the MCF10 progression series under 2D and 3D conditions with the top 50 siRNAs relative to NTC siRNA, depicting CREBBP, KMT2C, and NIPBL as 3D-specific hits. Bar chart of plate median normalized values for depicted genes are also shown. *, $P < 0.05$. **D,** Heatmap of the plate median normalized values of the validation screen of the spheroid viability of a panel of TNBC spheroids after siRNAs silencing of the top 50 genes identified from **B**. Common genomic alterations in the cell lines are depicted. **E,** Representative micrographs of H&E staining, and CREBBP and Ki-67 protein expression was evaluated by IHC from 7-day spheroids of MCF10DCIS.com. Text depicts Allred scores for CREBBP IHC and % Ki-67–positive cells. Scale bar, 200 μm.

all individual sequences resulted in a reduction in *CREBBP* mRNA and protein levels and an equivalent increase in spheroid size (Supplementary Fig. S2A–S2D). CREBBP-silenced spheroids displayed a reduction in CREBBP protein expression and concomitant increase in Ki-67 staining (**Fig. 1E**), suggesting that this increase in size was because of an increased proliferative capacity. Silencing of *CREBBP* with two distinct doxycycline-inducible shRNA hairpins increased MCF10DCIS.com spheroid growth after 14 days (Supplementary Fig. S2E), and was maintained up to 30 days, showing that that continued suppression of CREBBP expression results in a sustained increase in spheroid growth ($P < 0.05$, t test; Supplementary Fig. S2F).

CREBBP loss promotes growth under nutrient stress conditions, and leads to global acetylation differences and increased transcriptomic heterogeneity

Our findings, demonstrating CREBBP loss specifically promoted growth in 3D conditions, are in agreement with a recent study using whole-genome CRISPR screening in lung cancer, which also found CREBBP knockout had a marked 3D-specific increase on spheroid size (4). These results, hence suggest that environmental factors could impact its capacity as a tumor suppressor gene. Silencing of CREBBP in 2D culture under full-serum normoxic conditions resulted in a reduction of cell number, whereas cell viability was increased in CREBBP-silenced cells grown under low-serum conditions (**Fig. 2A**). Growth under both hypoxia and low-serum conditions showed a substantial increase in cell number relative to siControl cells (**Fig. 2A**), suggesting that both nutrient stress and hypoxia are required for CREBBP-silenced cells to acquire a growth advantage. The phenotypic effect of CREBBP was further confirmed in a CREBBPmut and WT isogenic cell line model derived from the haploid leukemia cell line, HAP1 (Supplementary Fig. S2G). HAP1 CREBBPmut cells had a marked 4-fold increase in cell viability and significant increase in spheroid volume ($P < 0.001$, t test), but a significantly lower cell viability in 2D culture in keeping with our

Published OnlineFirst January 28, 2021; DOI: 10.1158/0008-5472.CAN-20-1822

observations in the MCF10a cell lines, and thus highlighting the utility of this model (**Fig. 2B**).

CREBBP is a HAT that regulates the acetylation status of both histone and nonhistone proteins (34) and loss-of-function mutations drive B-cell lymphoma (BCL), small-cell lung cancer (SCLC), and pediatric acute lymphoblastic leukemias (35–38). We thus sought to characterize acetylation changes at the protein level induced by CREBBP mutations by using mass spectrometry in the HAP1 WT and CREBBPmut cell model due to the fact CREBBP loss had the largest phenotypic effect in this model. This analysis identified 52 internal acetylated and 267 N-terminal acetylated peptides mapping to known proteins that were detected in CREBBPmut and WT cells (Supplementary Table S4). Of these, two of 52 internal acetylated peptides were differentially expressed between CREBBPmut and WT cells, whereas 92 of 267 N-terminal acetylated peptides were differentially expressed in CREBBPmut cells compared with WT cells (FDR corrected $P < 0.1$, t test; Supplementary Table S4). These included dysregulation of internal acetylated peptides of the nonhistone proteins, including ZNF846 and HSP90AB1. The most significantly downregulated N-terminal lysine residues mapped to histone H3 (HIST3H3 and H3F3A), histone H2, and histone H4, in line with CREBBP's known function (**Fig. 2C**, **i**). Furthermore, pathway analysis of these differential N-terminal acetylated proteins highlighted histone deacetylase (HDAC) class III signaling (involved in the deacetylation of acetyl lysine substrates) to be the most significantly enriched pathway (Supplementary Table S4). In agreement with this, we identified that the majority (38/56, 68%) of all detected HDAC and HAT proteins showed a significant difference in total protein expression in CREBBPmut cells. These included a number of proteins with acetyltransferase and deacetylase activity (e.g., downregulation of HDAC4, 6, and 9, upregulation of HDAC1 and 2, as well as upregulation of a number of proteins with N-terminal de/acetylase activity; **Fig. 2C**, **ii**; Supplementary Table S4; including ESCO2 and the H2A- and H4-specific N-terminal transferase NAA40). As a consequence of HAT/HDAC dysregulation, cells were significantly more sensitive to the broad range HDAC inhibitors, tricostatin A and vorinostat, than WT cells (**Fig. 2D**). Taken together, these results indicate that loss of CREBBP results in global dysregulation of N-terminal acetylation of lysine acetylation modulators, suggesting an irreversible rewiring of epigenetic patterns that subsequently lead to changes in the total and phosphoproteome.

To further quantitatively assess whether loss of CREBBP led to diverse/global changes at the transcriptomic level, we performed single-cell RNA sequencing of CREBBPmut and WT HAP1 spheroids using the 10X Genomics platform. By performing unsupervised pseudotime reconstruction analysis to study the gene expression dynamics in heterogeneous cell populations (22), we found that CREBBPmut cells clustered into 11 distinct transcriptional states compared with seven in WT cells, suggesting loss of CREBBP results in global transcriptomic alterations, again in agreement with its known function (**Fig. 2E**). By overlaying the published "Buffa" hypoxia signature (39) onto these trajectories, we found that the CREBBPmut cells displayed a divergent response to hypoxia compared with WT cells, with WT cells showing a distinct canonical response to hypoxia as there was a single, but large subpopulation that showed an increase in hypoxic gene signature expression. In contrast, cells from CREBBPmut spheroids did not display transcriptional changes in response to hypoxia (**Fig. 2F**). Indeed, when we analyzed the protein expression of the proliferative marker Ki-67, CREBBPmut spheroids had sustained expression of Ki-67 toward the center of the sphere, while WT spheroids did not, suggesting that CREBBPmut cells were more able to proliferate under an unfavorable environment (**Fig. 2G**). Moreover, CREBBPmut spheroids displayed ubiquitous staining of the hypoxic marker, carbonic anhydrase IX (CAIX), whereas WT spheroids showed only an increase in CAIX toward the core, supporting the hypothesis that CREBBPmut spheroids are distinct in how they respond to low oxygen. As hypoxic cells heavily rely on glycolysis for energy production rather than lactate (as in normoxic cells), inhibition of monocarboxylase transporter 1 (MCT1), which controls bidirectional transport of lactate across the extracellular membrane, has been shown to preferentially kill hypoxic cells through glucose deprivation (40). Indeed, treatment with the MCT1 inhibitor, AZD3965, significantly reduced viability in CREBBPmut spheroids, while having no effect on WT spheroids (**Fig. 2H**). Together, these results suggest that loss of CREBBP induces hypoxia in cells and promotes their survival when they encounter nutrient stress and low oxygen conditions.

CREBBP protein expression is associated with a poor outcome in TNBC and protein loss is common in other tumor types that harbor CREBBP mutations

To investigate the clinical implications of *CREBBP* alterations in TNBC, we evaluated patient data from TCGA (1, 2) and Molecular Taxonomy of Breast Cancer International Consortium (METABRIC) cohorts (1, 41). The mutational frequency of *CREBBP* in breast cancer (TCGA) identified an enrichment of mutations in TNBCs, compared with ER^+ disease (**Fig. 3A**). In addition, heterozygous *CREBBP* copy-number losses were observed in 25%–33% of patients from TCGA, METABRIC, and Memorial Sloan Kettering Cancer Center (MSKCC) cohorts (**Fig. 3B**; refs. 1, 33, 41). Stratifying patients as WT or with *CREBBP* mutations and/or copy-number losses (CREBBPaltered) showed that CREBBPaltered tumors had a significant reduction in CREBBP mRNA expression ($P < 0.05$, t test; **Fig. 3C**), indicating a dose-dependent correlation between copy number and gene expression. Assessment of CREBBP protein expression on TMAs from two independent cohorts of TNBCs ($n = 174$) identified a reduction in CREBBP protein levels in 48.3% of TNBCs, with 20.1% showing either low or no CREBBP protein expression (11.5% low and 8.6% no expression, respectively; **Fig. 3D**). We also observed a significant correlation between CREBBP mRNA expression and protein expression, as detected by IHC ($P = 0.004$, Mann–Whitney U test; Supplementary Fig. S3A). TNBCs that had lower levels of *CREBBP* mRNA expression had a significantly reduced disease-specific–free survival (DSS), compared with high expressing tumors in the METABRIC cohort [$P = 0.021$, Wald test; hazard ratio, 0.48; 95% confidence interval (CI), 0.26–0.90, multivariable analysis; **Fig. 3E**]. Corroborating these results, a trend toward an association of reduced CREBBP protein levels and poorer distant metastasis-free survival (DMFS) was observed using IHC in patients with TNBC ($P = 0.11$, Wald test; hazard ratio, 0.52; 95% CI, 0.23–1.16, multivariable analysis; **Fig. 3F**). A significant association with DMFS was also observed at the mRNA level in the Belgrade cohort ($P = 0.04$, Wald test; hazard ratio, 0.48; 95% CI, 0.24–0.97, multivariable analysis; **Fig. 3G**).

Additional analysis of TCGA data identified that a considerable proportion of other solid tumors had a high frequency of alterations in *CREBBP*, including uterine, ovarian, squamous lung, and bladder cancers (Supplementary Fig. S3B). Moreover, protein assessment with IHC on TMAs of endometrial, squamous lung, bladder, and high-grade serous ovarian cancers identified a substantial proportion of these tumor types to have reduced CREBBP protein levels (Allred score < 4; Supplementary Fig. S3C), highlighting that loss of CREBBP protein expression is a recurrent alteration that occurs in multiple tumor types.

Published OnlineFirst January 28, 2021; DOI: 10.1158/0008-5472.CAN-20-1822

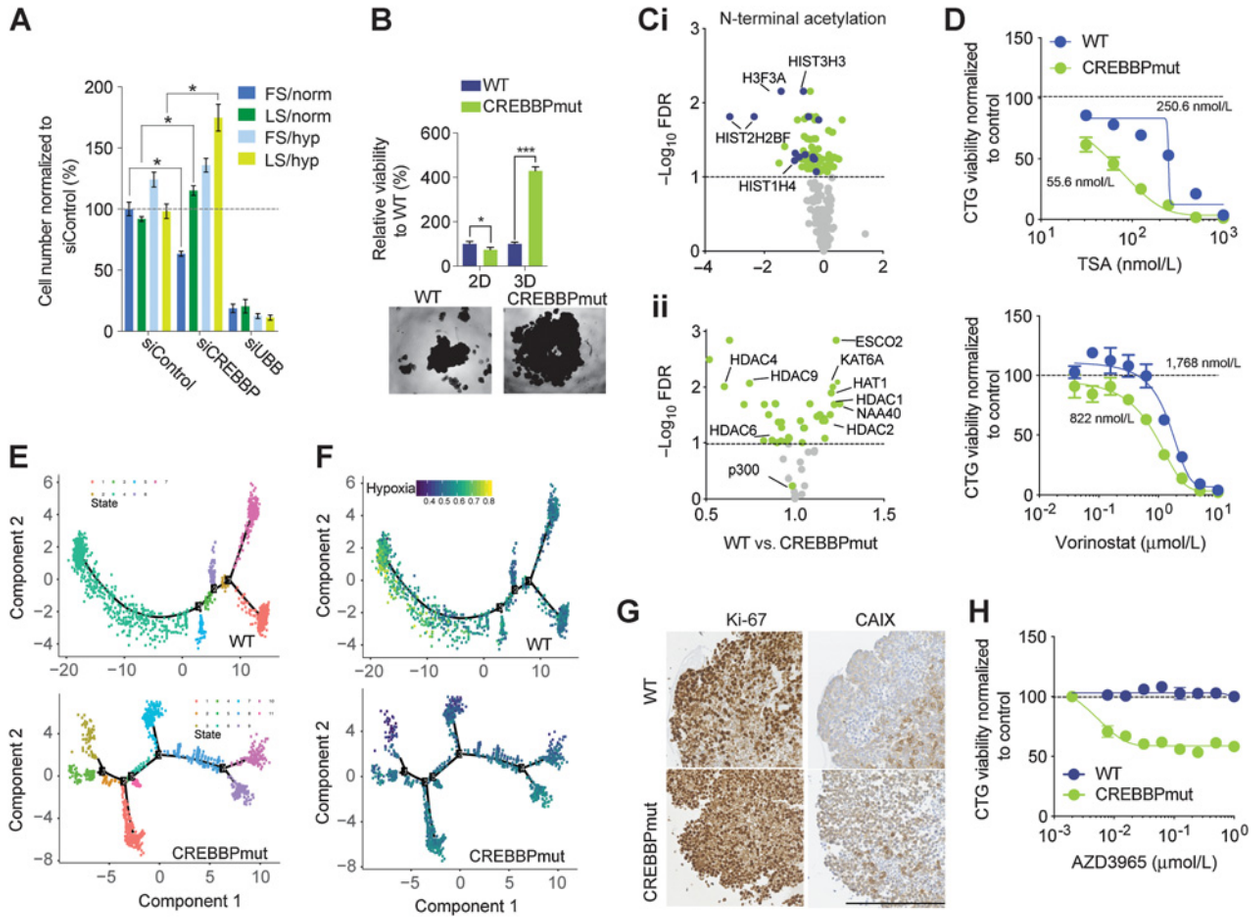

Figure 2.

CREBBP loss promotes growth under nutrient stress and hypoxia conditions and confers sensitivity to HDAC and MCT1 inhibition. **A,** Bar chart depicting normalized cell viability as assessed with CellTiter-Glo of MCF10AT1 cells that were grown in 2D under differing serum (full/10% and low/1% FBS) and oxygen (normoxia/20% and hypoxia/1% O^2) and in combination for 4 days. siUBB was used as a positive cell killing control. **B,** Bar chart representing isogenic HAP1 cell growth in 2D and 3D for 7 days. Representative bright-field images of WT and CREBBPmut spheroids are also shown. *, $P < 0.05$, ***, $P < 0.0001$. **C,** Volcano plot of the significantly altered N-terminal acetylated peptides between CREBBPmut and WT cells (**i**). HAP1 WT and CREBBPmut spheroids were grown for 5 days. Log_2-fold change is plotted against $-log_{10}$ of FDR corrected *P* value. Histone proteins are highlighted in blue. Volcano plot of fold change of total protein expression of histone acetylase and deacetylases plotted against FDR corrected *P* value (**ii**). **D,** Dose–response curves of HAP1 WT and CREBBPmut spheroids treated with increasing concentrations of HDAC inhibitors, tricostatin A (TSA) and vorinostat for 5 days. **E,** Single-cell RNA sequencing analysis after 7 days of growth. DDRTree visualization and 2D embedding showing constructed pseudotime transcriptional states for WT and CREBBPmut spheroid cells, depicting an increased number of branches in the CREBBPmut cells, indicative of differential transcriptional programs over time. **F,** Single-cell RNA sequencing from **E** was also analyzed for the presence of a hypoxia gene signature. **G,** Representative micrographs of CREBBP, Ki-67, and CAIX expression in HAP1 WT and CREBBPmut spheroids. Scale bar, 100 μm, indicating increased proliferation in CREBBPmut cells and increased levels of the hypoxia marker, CAIX. **H,** Dose–response curves of HAP1 WT and CREBBPmut spheroids treated with increasing concentrations of the selective MCT1 inhibitor, AZD3965, for 5 days, showing that CREBBPmut cells are selectively sensitive to MCT1 inhibition. Spheroid viability was assessed using CellTiter-Glo and normalized to DMSO-treated cells. FS/norm, full-serum normoxic; FS/hyp, full-serum hypoxia; LS/norm, low-serum condition; LS/hyp, hypoxia and low-serum condition.

Recent data have highlighted the importance of cellular phenotypic heterogeneity in therapeutic resistance in ER^+ breast cancer mediated through disrupted expression in the lysine deacetylase protein, KDM5 (24). Akin to this, we hypothesized that alterations in CREBBP may also lead to changes in tumor heterogeneity in TNBC. Indeed, patients with CREBBP alterations displayed a higher transcriptional diversity at the gene, isoform, and exon level ($P < 0.01$, Welch *t* test) and higher mutational burden (**Fig. 3H** and **I**; Supplementary Fig. S3D). These observations suggest that CREBBP status in patients influences transcriptomic heterogeneity, a known factor, that may determine treatment response (42), in keeping with our observed correlations with a poor patient outcome.

CREBBP alterations lead to increased proliferation via FOXM1 expression and activity and are selectively sensitive to CDK4/6is

To elucidate altered pathways driving the aggressive nature of CREBBPaltered TNBCs, we compared the transcriptomic profiles and reverse phase protein array (RPPA) proteomic profiles from patients with CREBBPaltered TNBC with and without CREBBP alterations (WT) from TCGA. In total 1,062 transcripts and 21 proteins (total or phosphorylated) were significantly up- or downregulated in CREBB-Paltered TNBCs (**Fig. 4A**; Supplementary Table S5). Common pathways enriched at both the gene expression and protein level in CREBBPaltered TNBCs identified the oncogenic FOXM1

Published OnlineFirst January 28, 2021; DOI: 10.1158/0008-5472.CAN-20-1822

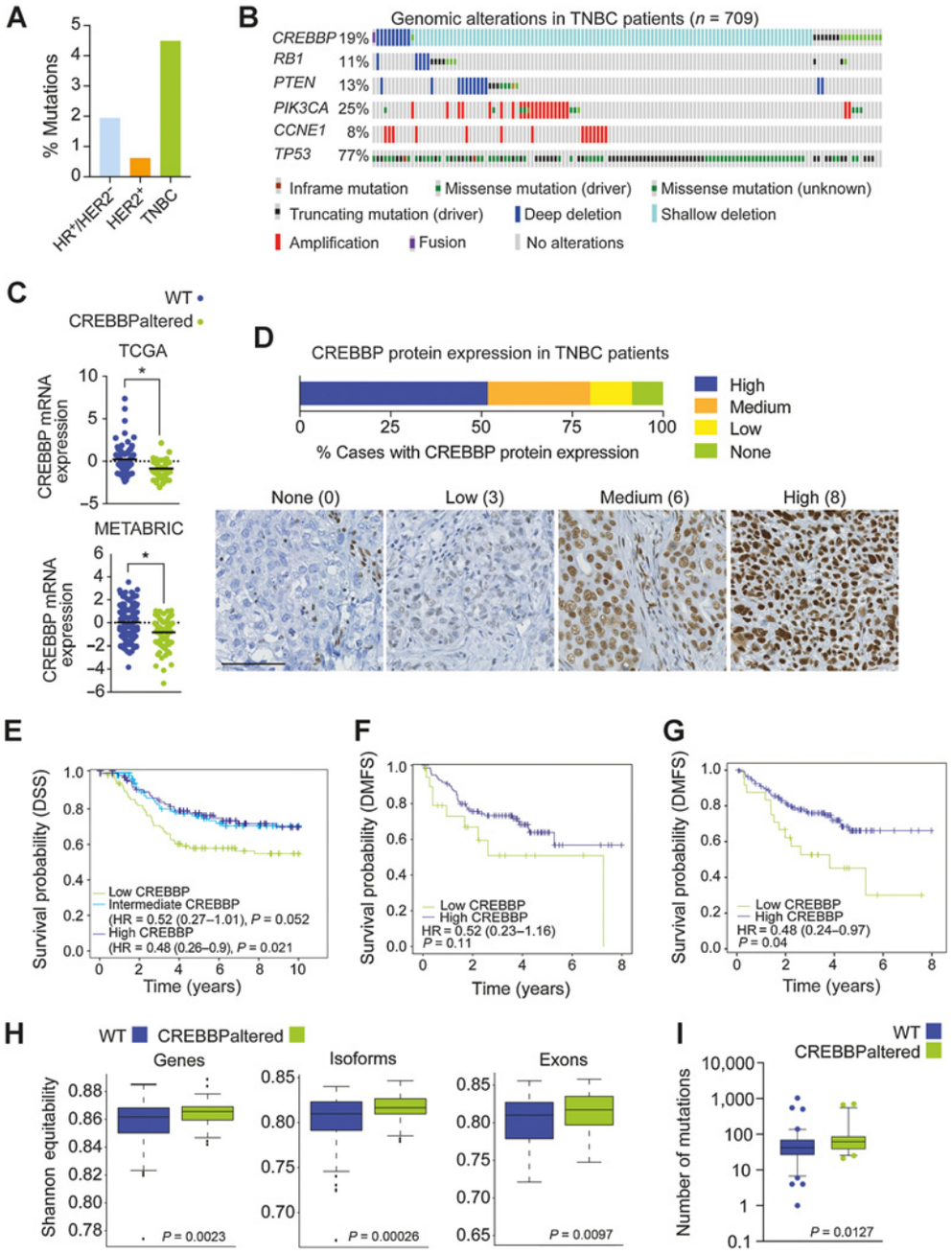

Figure 3.

CREBBP protein expression is associated with a poor prognosis in TNBC. **A,** Frequency plot of *CREBBP* mutations in breast cancer (from TCGA) stratified on subtype. **B,** OncoPrint plot of genomic alterations in *CREBBP* in a combined analysis of TNBC ($n = 709$) from TCGA, METABRIC, and MSKCC cohorts. Frequencies of additional genomic alterations in TNBC are also depicted. **C,** *CREBBP* mRNA expression in TNBCs stratified on CREBBP status in TCGA and METABRIC. *, $P < 0.05$. **D,** Bar chart depicting frequency of CREBBP protein expression in TNBCs from TMAs of the Belgrade and BR10011a cohorts combined ($n = 174$). Representative micrographs of CREBBP protein expression are shown from Belgrade cohort and corresponding Allred scores. Scale bar, 100 μm. **E,** Kaplan–Meier plots for DSS in TNBCs from METABRIC cohort ($n = 276$) and were stratified on their *CREBBP* mRNA expression (high, intermediate, and low). Multivariable survival analysis was performed by taking into account *CREBBP* mRNA expression status, age, tumor size, node status, and grade. **F,** Kaplan–Meier plots for DMFS in TNBCs that were stratified on their CREBBP protein expression (high and low) from the Belgrade cohort that had associated outcome data. Low CREBBP expression was defined as Allred score < 4. Multivariable survival analysis was performed by taking into account CREBBP protein expression status, age, tumor–node–metastasis (TNM) stage, and grade. **G,** Kaplan–Meier plots for DMFS in TNBCs that were stratified on their *CREBBP* mRNA expression (high and low) from the Belgrade cohort that had associated outcome data. Multivariable survival analysis was performed by taking into account *CREBBP* mRNA expression status, age, TNM stage, and grade. **H,** Box plots of the diversity of gene, isoform, and exon expression in CREBBP WT and CREBBPaltered TNBCs. Diversity index was calculated using Shannon equitability index. **I,** Box plots of the mutational burden in CREBBP WT and CREBBPaltered TNBCs.

Published OnlineFirst January 28, 2021; DOI: 10.1158/0008-5472.CAN-20-1822

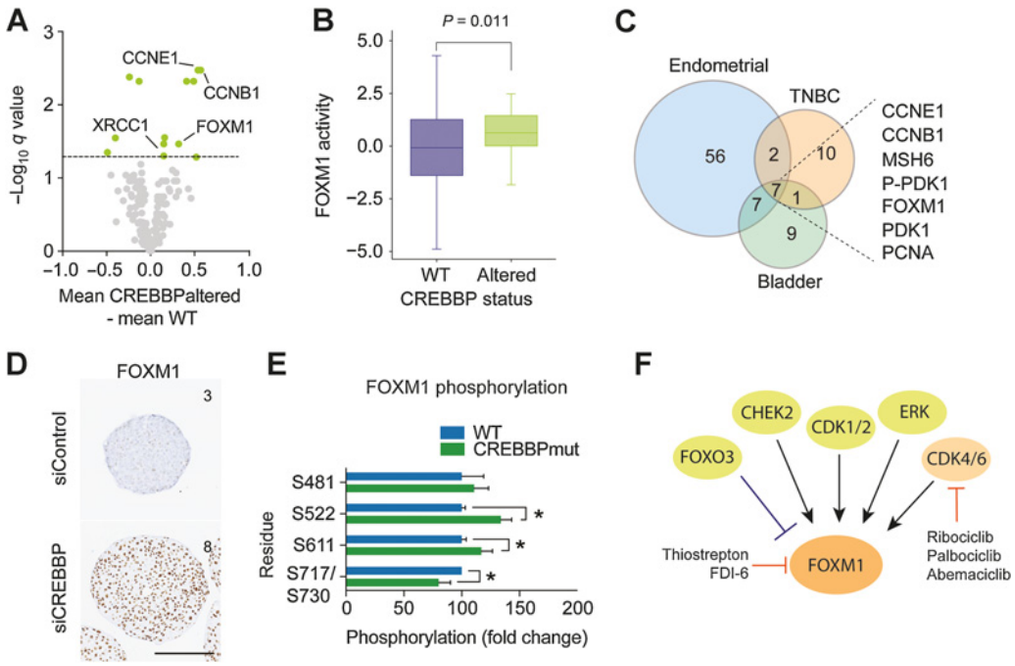

Figure 4.

CREBBPaltered cancers show increased FOXM1-driven proliferation. **A,** Volcano plot of fold change in protein expression (*x*-axis) from RPPA data of TNBCs stratified on CREBBP status, plotted against −log10 *P* value (*y*-axis). Significant alterations in protein expression are highlighted in orange (FDR corrected $P < 0.1$). **B,** Box plot of *FOXM1* gene activity in CREBBPaltered TNBC. mRNA expression from TCGA was used to calculate FOXM1 activity utilizing a rank-based enrichment analysis (see Supplementary Materials and Methods). **C,** Venn diagram of significantly altered proteins between CREBBPaltered and WT tumors from RPPA data of TNBCs, endometrial cancers, and bladder cancers. **D,** Representative micrographs of FOXM1 protein expression from 7-day spheroids of MCF10DCIS.com after siRNA silencing of CREBBP or NTC. Text depicts IHC quantification (Allred scores). Scale bar, 200 μm. **E,** Bar plot of fold change in phosphorylated protein expression (*x*-axis) from mass spectrometry assessment of day 4 spheroids of HAP1 WT and CREBBPmut spheroids, plotted against $-\log_{10} P$ value (*y*-axis). *, $P < 0.05$. **F,** A diagram of FOXM1 and the proteins that regulate its activity. Direct and indirect inhibitors are highlighted.

transcription factor network to be the most significantly enriched pathway in CREBBPaltered tumors (protein level q value = 7.01E-9 and transcript level q value = 2.28E-6). This unbiased analysis also identified enrichment of a number of pathways involving G_1–S-phase cell-cycle control (Supplementary Fig. S4A; ref. 43), highlighting that in patients with TNBC CREBBP alterations lead to increased proliferation, in keeping with our observations *in vitro*. Further analysis of TCGA patient RNA sequencing data by using unbiased transcription factor activity module analysis (30) also highlighted that CREBBPaltered TNBCs showed significantly higher FOXM1 transcriptional activity ($P = 0.011$, *t* test; **Fig. 4B**). FOXM1, and known downstream targets were also significantly upregulated at the protein level in bladder and endometrial cancers with genomic alterations in *CREBBP*, demonstrating that increased proliferation is a general feature of CREBBPaltered tumors (q value < 0.05; **Fig. 4C**; Supplementary Fig. S4B and S4C). FOXM1 upregulation was further validated in CREBBP-silenced MCF10DCIS.com spheroids (**Fig. 4D**), as well as HAP1 CREBBPmut cells (Supplementary Fig. S4D) by using IHC. Assessment of the phosphoproteome of WT and CREBBPmut spheroids highlighted a significant increase in FOXM1 phosphorylation on residues S522 and S611 in CREBBPmut spheroids (Supplementary Table S4), which are two sites that have been shown to be exclusively regulated by CDK4/6 (**Fig. 4E**; ref. 20). In addition, we identified an enrichment of CDK4 and CDK6 kinase motifs in the CREBBPmut spheroids, suggesting that loss of CREBBP leads to enhanced CDK4 and CDK6 activity (Supplementary Fig. S4E; refs. 20, 21).

FOXM1 can be indirectly targeted through suppression of CDK4/6 phosphorylation sites using CDK4/6i (**Fig 4F**; ref. 20). Indeed, treatment of WT and CREBBPmut spheroids with three structurally distinct clinical CDK4/6is (ribociclib, palbociclib, and abemaciclib) demonstrated a marked increase in sensitivity in CREBBPmut cells compared with WT cells (CREBBPmut SF50 were 180, 434, and 1,594 nmol/L and WT SF50 were >10, 6.4, and >10 μmol/L for palbociclib, abemaciclib, and ribociclib, respectively; **Fig. 5A**). No difference was observed in sensitivity upon treatment with the CDK2/7/9 inhibitor, SNS-032, highlighting the specificity of targeting CDK4 and CDK6 in these cells. Confirming our phosphoproteomic analysis, we observed an increase in FOXM1 phosphorylation (S35) in CREBBPmut spheroids, which was reduced with exposure to the CDK4/6i, palbociclib, in CREBBPmut spheroids, while little effect was detected in WT spheroids (**Fig. 5B**). Treatment of cells with CDK4/6i also led to a concomitant decrease in cyclin B protein expression, and reduced mRNA expression of known direct FOXM1 target genes *AURKB, CCNB1, CCNE1, CDC25C*, and *CENPF* (**Fig. 5C**), demonstrating that CDK4/6i could selectively target the proliferative transcriptional activity of FOXM1 in CREBBPaltered cells. We further validated the CREBBP/CDK4/6i association in a histologically diverse panel of tumor cell lines. Compared with WT cell lines (lung: A549 and H1299 and colon: HCT116), additional *CREBBP*-mutant lung, endometrial, leukemia, and BCL cell lines (NCI-H520, AN3CA, NALM-6, SU-DHL-6, and NU-DHL-1) were significantly more sensitive to palbociclib ($P = 0.0099$, *t* test), indicating that this effect is likely not restricted to cancer cells

Published OnlineFirst January 28, 2021; DOI: 10.1158/0008-5472.CAN-20-1822

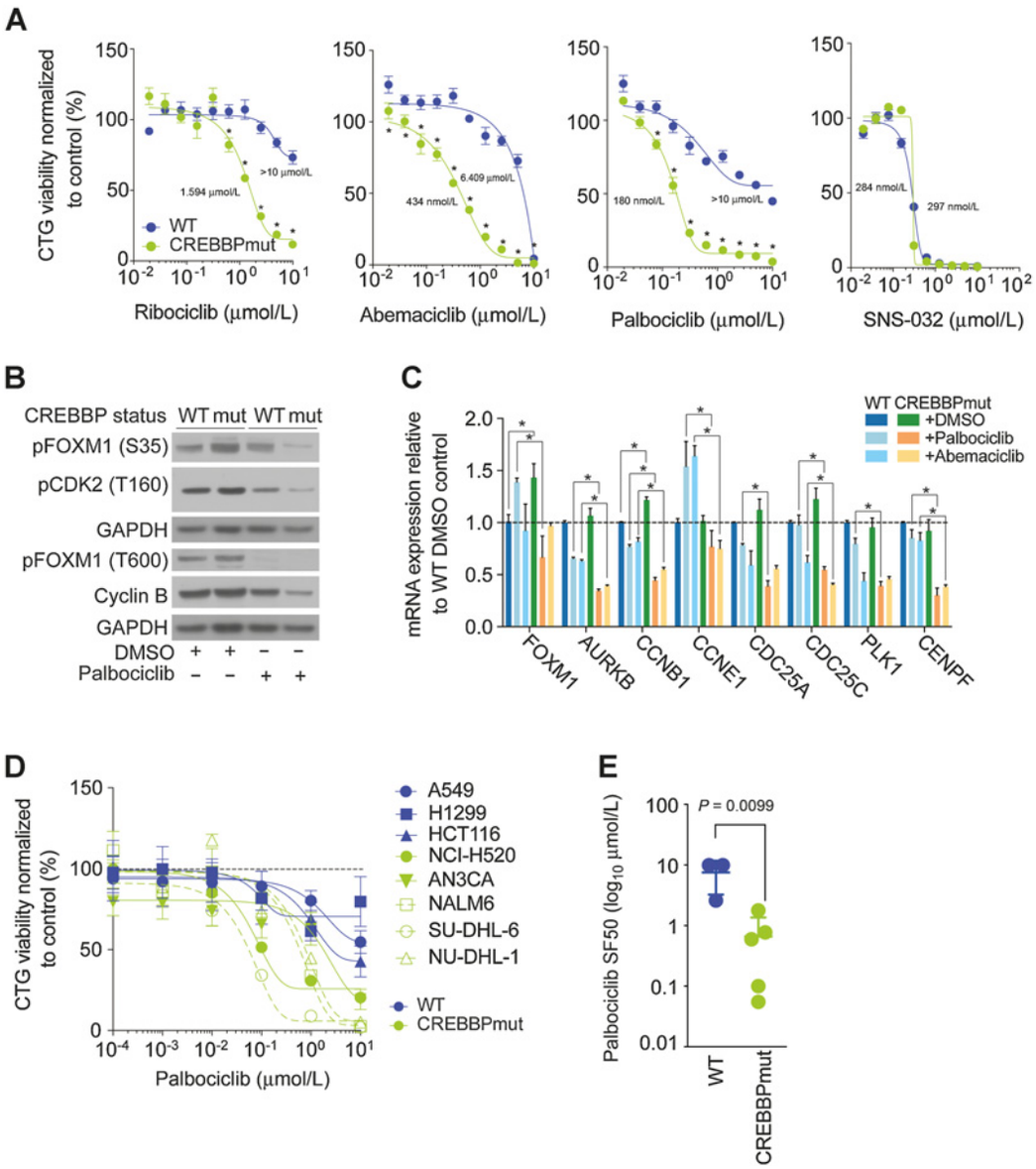

Figure 5.

CREBBP loss sensitizes cells to CDK4/6i. **A,** Dose–response curves of HAP1 WT and CREBBPmut cells treated with increasing concentrations of the clinical CDK inhibitors, ribociclib, abemaciclib, palbociclib, and SNS-032 at the concentrations indicated. **B,** Western blot analysis of protein lysates of HAP1 WT and CREBBPmut cells treated with 1 μmol/L of palbociclib or DMSO for 48 hours showing suppression of specific phospho sites in CREBBPmut cells. **C,** Bar chart of relative mRNA expression of FOXM1 target genes in HAP1 WT and CREBBPmut cells +/− palbociclib (250 nmol/L), abemaciclib (500 nmol/L), or DMSO treatment at 24 hours after cell seeding for 72 hours. Gene expression was quantified using RT-PCR. **D,** Dose–response curves of a panel of nonisogenic cancer cell lines (WT: lung, A549 and H1299 and colorectal, HCT116; and CREBBPmut: lung, NCI-H520; endometrial, AN3CA; leukemia, NALM-6; and lymphoma, SU-DHL-6 and NU-DHL-1) spheroids treated with increasing concentrations of palbociclib for 5 days and displayed according to CREBBP status. **E,** Bar chart of SF50 values of nonisogenic CREBBPmut and WT cell lines grown as spheroids and treated with palbociclib for 5 days. *, $P < 0.05$.

from just one tumor type (**Fig. 5D** and **E**). In addition, in TNBC cell lines, where CREBBP silencing leads to increased growth, it also induced a greater sensitivity to palbociclib compared with the NTC (Supplementary Fig. S5A). In line with the 3D-specific effect of CREBBP silencing on growth, we also found that sensitivity to CDK4/6i was specific to spheroid cultures (Supplementary Fig. S5B–S5D).

CREBBPaltered cells show selective sensitivity to CDK4/6is *in vivo*

We next assessed whether the clinically approved CDK4/6i, palbociclib, could inhibit CREBBPaltered tumors *in vivo*. To do this, we generated cohorts of mice with established xenograft tumors derived from either the high-grade lymphoma cell line SU-DHL-6 that harbors an inactivating frameshift mutation (L470*) in CREBBP (36) or the

Published OnlineFirst January 28, 2021; DOI: 10.1158/0008-5472.CAN-20-1822

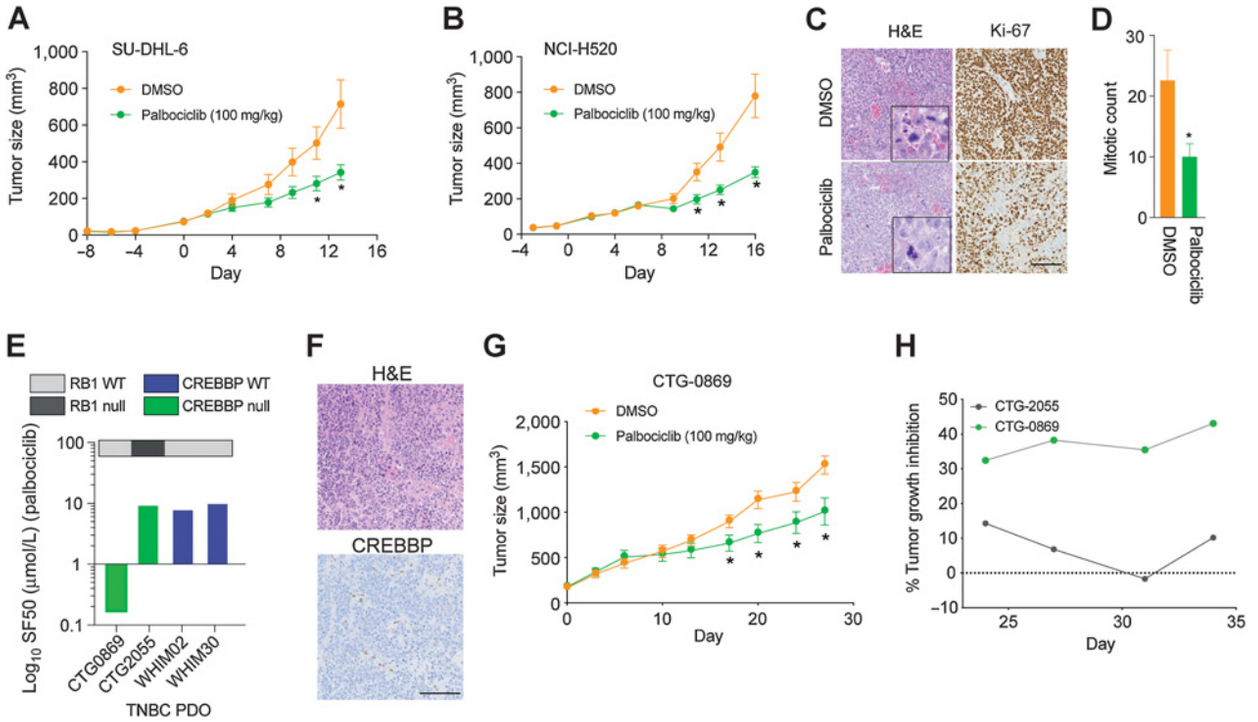

Figure 6.

CREBBPaltered tumors are sensitive to CDK4/6i *in vivo*. **A,** Chart depicting tumor volume of the therapeutic response to palbociclib treatment in immunocompromised mice bearing CREBBPmut SU-DHL-6 tumors over time. Tumor volumes after the initiation of treatment are shown. *, $P < 0.05$. **B,** Chart depicting tumor volume of the therapeutic response to palbociclib treatment in immunocompromised mice bearing CREBBPmut NCI-H520 tumors over time. Tumor volumes after the initiation of treatment are shown. **C,** IHC staining of representative tumors harvested from CREBBPmut NCI-H520 tumors for Ki-67 and H&E staining. Scale bar, 100 μm. **D,** Bar chart showing the quantification of mitotic counts in palbociclib- and control-treated animals from **C**. **E,** Bar chart depicting SF50 values of palbociclib in a panel of TNBC PDOs. CREBBP and RB1 status are shown. **F,** Representative micrographs of H&E staining and CREBBP protein expression of the TNBC PDX CTG-0869 depicting protein loss of CREBBP. Scale bar, 100 μm. **G,** Chart depicting CTG-0869 tumor volume of the therapeutic response to palbociclib treatment in immunocompromised mice. Tumor volumes after the initiation of treatment are shown. **H,** Chart depicting tumor growth inhibition as percentage of DMSO-treated mice bearing CTG-0869 and CTG-2055 TNBC xenografts treated with palbociclib at 100 mg/mL after 3 weeks of treatment until experiment endpoint.

aggressive lung squamous cell carcinoma cell line NCI-H520, which harbors the recurrent CREBBP hotspot mutation R1446C, resulting in inactivation of HAT domain activity (44). Continuous treatment of tumors with palbociclib (100 mg/kg) daily for 14–16 days had a marked effect on tumor growth and weight ($P < 0.05$, *t* test; **Fig. 6A** and **B**) and significant increase in survival ($P = 0.0178$, SU-DHL-6 and $P = 0.0002$, NCI-H520; Supplementary Fig. S6A–S6E). Palbociclib-treated tumors displayed a significant reduction in the proliferative fraction of the tumor measured by Ki-67 expression ($P = 0.0089$, *t* test) and mitotic index ($P = 0.0160$, *t* test; **Fig. 6C** and **D**). To model the clinical scenario, a chemotherapy pretreated TNBC (CTG-0869) patient-derived organoid (PDO) negative for CREBBP protein expression that showed no clinical response to docetaxel or capecitabine/bevacizumab, grown *ex vivo* was sensitive to palbociclib treatment (SF50 = 160 nmol/L; **Fig. 6E**), whereas CREBBP-null RB1-deficient and CREBBP WT RB1-proficient TNBC PDOs were not (**Fig. 6E**; Supplementary Fig. S7). Treatment of the CREBBP-null RB1-proficient model CTG-0869 grown *in vivo* also showed a significant reduction in tumor growth and extended survival, an effect that was superior to the chemotherapy gemcitabine (**Fig. 6F**–**H**; Supplementary Fig. S8A–S8C). Moreover, palbociclib treatment of an additional CREBBP-null RB1-null TNBC patient-derived xenograft (PDX) CTG-2055 *in vivo* showed no response (Supplementary Fig. S8D). Together, our results demonstrate that *CREBBP* is a novel tumor suppressor gene in TNBC and suggest that CDK4/6i could have potential as treatments for aggressive CREBBPaltered cancers, which have failed standard treatment.

Discussion

Our approach using 3D spheroid models to identify novel cancer drivers identified a number of genes not previously implicated in TNBC pathogenesis. Our data deconvoluting the phenotypic effect of CREBBP silencing suggest that this is likely to be regulated via hypoxia and nutrient stress. This is in keeping with recent studies demonstrating that histone demethylases directly sense oxygen to control chromatin and cell fate (45). It is thus likely that additional histone acetylases and deacetylases also have similar oxygen sensing roles. Our data are in agreement with a recent pan-cancer analysis study that highlighted *CREBBP* mutations to be one of the most highly correlated mutated genes in tumors with elevated hypoxic signatures (46). In addition, in support of our overall approach, a recent unbiased 3D CRISPR loss-of-function screen in lung cancer cell line spheroids identified an enrichment of genes that had 3D-specific phenotypic effects that more closely mirrored *in vivo* phenotypes. Moreover, these were highly enriched for commonly mutated genes in lung cancer, including *CREBBP* (4). This is in keeping with studies in genetically engineered mouse models that have also highlighted that *CREBBP*

deletions enhance tumorigenesis in BCL and SCLC models (35, 47) and suggest that CREBBP inhibitors currently being tested in patients may not have clinical utility to treat these cancers (48).

Recent studies have demonstrated synthetic lethal interactions between CREBBP and its orthologue EP300, highlighting the potential utility of EP300 inhibitors for CREBBP-deficient tumors (49). In addition, HDAC inhibitors have been shown to be effective in *CREBBP*-mutant tumors, which act via restoration of acetylation and expression of cellular adhesion proteins and increased dependency on HDAC3 (47). Our data also suggest that changes in N-terminal acetylation of proteins involved in HDAC3 activity may lead to increased sensitivity to HDAC inhibition through resultant increase in expression of multiple HDAC proteins as consequence of CREBBP loss. However, in our models, we found that the CREBBP/CDK4/6i selectivity was more profound than these other proposed CREBBP-targeted agents, highlighting that the effect with HDAC inhibitor may have less efficacy in patients.

In agreement with the loss-of-function mutation of other epigenetic modulators (24), we identified *CREBBP* alterations to result in higher transcriptional heterogeneity while maintaining a capacity for cells to survive under nutrient stress conditions, that is, those that you would find in tumors that display hypoxia and have a poor prognosis. This phenotype was validated in patients with CREBBPaltered TNBC, where *CREBBP* mutations or copy-number losses resulted in a greater transcriptional diversity. Thus, we propose a model whereby CREBBP loss imparts a more aggressive disease trajectory in TNBC as a result of increased transcriptomic diversity. This is in agreement with the clinical observations that CREBBPaltered tumors are less sensitive to established anticancer therapies and patients are more likely to relapse. Interestingly, *CREBBP* mutations have been found to be enriched in metastatic ER^+ breast cancers, suggesting a role in therapy resistance in agreement with our data in TNBC (33). We identified a substantial proportion of patients with depletion of CREBBP expression through IHC assessment across multiple tumor cohorts represented on TMAs, including endometrial, bladder, ovarian, and squamous lung cancer. For instance, only 8% of squamous lung cancers are known to harbor mutations in *CREBBP* (3), however, we observed protein depletion in up to 73% of cases, suggesting multiple mechanisms exist associated with reduced expression (3). This highlights that protein loss may be useful for patient stratification in the context of biomarker-driven clinical trials, and demonstrates that alterations of *CREBBP* are common in multiple aggressive cancers.

To date CDK4/6is are licensed for use in metastatic ER^+ breast cancer and not used in TNBC, but their clinical efficacy is thought to be dependent on a functional RB axis (50), and in the context of TNBC and squamous cell lung cancers, RB1 inactivation is relatively common (1, 3). Although our *in vitro* and *in vivo* data suggest a functional RB1 axis is also required for response in TNBC, the majority of CREBBPaltered TNBCs (78%) and squamous lung cancers (79%) harbor a functional RB1 axis. In addition, there is some evidence to suggest that CDK4/6 can drive FOXM1-mediated transcription in the absence of RB1 (20, 51, 52). For instance, silencing of RB1 in FOXM1-amplified osteosarcoma patient-derived cells *in vivo* did not reverse CDK4/6i sensitivity, suggesting that in the context of FOXM1 amplification, CDK4/6 inhibition is effective even in the absence of RB1. These data suggest that other mechanisms of FOXM1 upregulation outside the context of CREBBP loss can also sensitize cells to CDK4/6i (52). Of note, we observed only 22% of RB1 loss-of-function alterations or CCNE1 amplifications (known mechanisms of resistance to CDK4/6i) in patients with CREBBPaltered TNBC.

In summary, the results from our study demonstrate that CREBBP alterations impart a survival advantage for cancer cells via enhanced proliferation. This is mediated through global changes in acetylation and subsequent transcriptional alterations, including upregulation of the FOXM1 proliferative signaling axis. As a consequence, this increased proliferative capacity renders CREBBPaltered cells sensitive to CDK4/6 inhibition, via inhibition of CDK4/6-mediated FOXM1 phosphorylation; a synthetic lethal association that was demonstrated in multiple tumor types both *in vitro* and *in vivo*. The highly recurrent nature of CREBBP alterations in treatment-resistant TNBC, lung cancer, bladder cancer, and lymphomas and the availability of FDA-approved CDK4/6i suggest this clinically translatable approach could benefit a wide range of patients with cancer as single agent or in combination with immunotherapeutic or other targeted approaches. Indeed, proof-of-concept trials, such as NCT03130439, which are evaluating the efficacy of single-agent abemaciclib in RB1-proficient TNBC will be crucial to interpreting our results further. Of note, although a recent phase II study in squamous lung cancers testing single-agent palbociclib in CCND1-, CCND2-, CCND3-, or CDK4-amplified patients failed to demonstrate the prespecified criteria for advancement to phase III, data from TCGA suggest only a small overlap between these alterations and CREBBP mutations, indicating the population may have been missed in the study (53).

Recent data have suggested that the use of CDK4/6i induces an intratumoral T-cell inflammatory signature that results in an enhanced response to PD-L1 (54, 55). Of note, we observed a significantly higher tumor mutational burden (a known biomarker of immunotherapy response) in patients with CREBBPaltered TNBC, bladder cancer, and squamous lung cancer, as well as in a pan-cancer analysis. The mechanism behind this increased mutational burden is unclear, but may be an indirect consequence of survival in hypoxic environments, which has been linked with downregulation of effective DNA repair mechanisms and accumulation of mutations (56). Although it is tempting to speculate that CREBBPaltered tumors may respond well to combinations of immune checkpoint blockade and CDK4/6i treatments, this needs to be tested in the clinical trial setting. However, our data provide the rationale for a molecularly stratified clinical trial.

Authors' Disclosures

S. Susnjar reports grants from Ministry of Education Science and Technology of Serbia during the conduct of the study. S. Pancholi reports grants from Breast Cancer Now during the conduct of the study. L.-A. Martin reports grants from Breast Cancer Now, Pfizer, Radius Health, AstraZeneca, and CRUK and personal fees from Pfizer during the conduct of the study and outside the submitted work. M.C.U. Cheang reports other from NanoString Technologies outside the submitted work, as well as has a patent for breast cancer classifier: US patent no. 9,631,239 with royalties paid with NanoString/Veractye. S. Postel-Vinay reports grants from Institute Roche, Boehringer Ingelheim, and Merck KGAa outside the submitted work, as well as has clinical activity in a drug development department where she is principal investigator or subinvestigator of clinical trials sponsored by the following companies: AbbVie, Adaptimmune, Aduro Biotech, Agios Pharmaceuticals, Amgen, Argen-X Bvba, Arno Therapeutics, Astex Pharmaceuticals, AstraZeneca Ab, Aveo, Basilea Pharmaceutical International Ltd, Bayer Healthcare Ag, Bbb Technologies Bv, BeiGene, Blueprint Medicines, Boehringer Ingelheim, Boston Pharmaceuticals, Bristol Myers Squibb, Ca, Celgene Corporation, Chugai Pharmaceutical Co, Clovis Oncology, Cullinan-Apollo, Daiichi Sankyo, Debiopharm, Eisai, Eisai Limited, Eli Lilly, Exelixis, Forma Therapeutics, GamaMabs, Genentech, GlaxoSmithKline, H3 Biomedicine, Hoffmann La Roche Ag, Imcheck Therapeutics, Innate Pharma, Institut De Recherche Pierre Fabre, Iris Servier, Janssen Cilag, Janssen Research Foundation, Kyowa Kirin Pharm. Dev, Lilly France, Loxo Oncology, Lytix Biopharma As, Medimmune, Menarini Ricerche, Merck Sharp & Dohme Chibret, Merrimack Pharmaceuticals, Merus, Millennium Pharmaceuticals, Molecular Partners Ag, Nanobiotix, Nektar Therapeutics, Novartis Pharma, Octimet Oncology Nv, Oncoethix, Oncopeptides, Orion Pharma, Ose Pharma, Pfizer, PharmaMar, Pierre

Fabre, Medicament, Roche, Sanofi Aventis, Sotio A.S, Syros Pharmaceuticals, Taiho Pharma, Tesaro, and Xencor. A.N. Tutt reports other funding from AstraZeneca, Merck KGAA, personal fees from Pfizer, Vertex, Artios, Prime Oncology, Inbiomotion, CRUK, MD Anderson, and Medscape Education, other funding from Medivation, Myriad Genetics, and AstraZeneca, grants from Breast Cancer Now Charity, CRUK, and AstraZeneca during the conduct of the study, honorarium from Merck, educational grant outside the submitted work, as well as has a patent for AstraZeneca with royalties paid by Institute of Cancer Research. R. Natrajan reports grants and nonfinancial support from Pfizer during the conduct of the study, as well as has a patent for UK IPO PCT/EP2018/065349 issued to WO/2018/228990. No disclosures were reported by the other authors.

Authors' Contributions

B. Peck: Conceptualization, formal analysis, supervision, investigation, methodology, writing-original draft, project administration, writing-review and editing. **P. Bland:** Data curation, formal analysis, project administration, writing-review and editing. **I. Mavrommati:** Data curation, formal analysis, validation, investigation, writing-review and editing. **G. Muirhead:** Data curation, software, formal analysis, visualization, writing-review and editing. **H. Cottom:** Investigation, writing-review and editing. **P.T. Wai:** Investigation, writing-review and editing. **S.L. Maguire:** Formal analysis, writing-review and editing. **H.E. Barker:** Investigation, writing-review and editing. **E. Morrison:** Investigation, writing-review and editing. **D. Kriplani:** Investigation, writing-review and editing. **L. Yu:** Investigation, writing-review and editing. **A. Gibson:** Investigation, writing-review and editing. **G. Falgari:** Investigation, writing-review and editing. **K. Brennan:** Resources, writing-review and editing. **G. Farnie:** Resources, writing-review and editing. **R. Buus:** Resources, data curation, investigation, writing-review and editing. **R. Marlow:** Resources, data curation, investigation, writing-review and editing. **D. Novo:** Resources, investigation, writing-review and editing. **E. Knight:** Resources, data curation, investigation, writing-review and editing. **N. Guppy:** Data curation, investigation, writing-review and editing. **D. Kolarevic:** Resources, data curation, formal analysis, investigation, writing-review and editing. **S. Susnjar:** Resources, data curation, formal analysis, validation, writing-review and editing. **N. Medic Milijic:** Resources, writing-review and editing. **K. Naidoo:** Resources, data curation, investigation, writing-review and editing. **P. Gazinska:** Data curation, formal analysis, investigation, methodology, writing-review and editing. **I. Roxanis:** Data curation, formal analysis, validation, writing-review and editing. **S. Pancholi:** Resources, investigation, methodology, writing-review and editing. **L.-A. Martin:** Resources, validation, writing-review and editing. **E.M. Holgersen:** Formal analysis, methodology, writing-review and editing. **M.C.U. Cheang:** Formal analysis, supervision, writing-review and editing. **F. Noor:** Formal analysis, investigation, methodology, writing-review and editing. **S. Postel-Vinay:** Formal analysis, supervision, validation, writing-review and editing. **G. Quinn:** Formal analysis, investigation, methodology, writing-review and editing. **S. McDade:** Data curation, software, formal analysis, supervision, writing-review and editing. **L. Krasny:** Resources, formal analysis, investigation, methodology, writing-review and editing. **P. Huang:** Formal analysis, supervision, investigation, writing-review and editing. **F. Daley:** Resources, supervision, investigation, methodology, writing-review and editing. **F. Wallberg:** Conceptualization, resources, data curation, software, formal analysis, supervision, funding acquisition, investigation, visualization, methodology, writing-original draft, project administration, writing-review and editing. **J.S. Choudhary:** Resources, data curation, supervision, investigation, methodology, writing-review and editing. **S. Haider:** Conceptualization, resources, data curation, software, formal analysis, supervision, funding acquisition, investigation, visualization, methodology, writing-original draft, project administration, writing-review and editing. **A.N. Tutt:** Resources, supervision, investigation, writing-review and editing. **R. Natrajan:** Conceptualization, data curation, formal analysis, supervision, funding acquisition, investigation, visualization, methodology, writing-original draft, project administration, writing-review and editing.

Acknowledgments

This work was funded by Programme grants from Breast Cancer Now as part of Programme Funding to the Breast Cancer Now Toby Robins Research Centre (to B. Peck, P. Bland, G. Muirhead, S.L. Maguire, D. Kriplani, A. Gibson, R. Marlow, R. Buus, D. Novo, E. Knight, N. Guppy, P. Gazinska, I. Roxanis, L.-A. Martin, E.M. Holgersen, F. Noor, F. Daley, F. Wallberg, S. Haider, A.N. Tutt, and R. Natrajan) and by funding from Breast Cancer Now's Catalyst Programme (grant Ref: 2018NovPR100 to I. Mavrommati and R. Natrajan), which is supported by funding from Pfizer; The Institute of Cancer Research (to G. Falgari, P.T. Wai, L. Yu, J.S. Choudhary, and R. Natrajan); MRC Confidence in Concept award (to R. Natrajan); Breast Cancer Now PhD studentship (2013NovPhD185 to E. Morrison); NC3Rs NC/P001262/1 (to A.N. Tutt); and Breast Cancer Now project grant (2014NovPR36 to L. Krasny and P. Huang). PDO generation was funded by Programme Grant funding to A.N. Tutt from Breast Cancer Now (CTR-Q4) as part of funding to the Breast Cancer Now Toby Robins Research Centre. ICR private donations funds were used to support the PDO work (to R. Marlow and A.N. Tutt). In addition, the Breast Cancer Now Research Unit at King's College London obtained funding from the National Institute for Health Research Biomedical Research Centre based at Guy's and St Thomas' NHS Foundation Trust and King's College London (to A.N. Tutt). We thank Charlotte Ng for input into generation of the gene list. We thank Charles Mein, Eva Wozniak, and Hothri Ananyambica Moka at the Barts sequencing facility for running the single-cell RNA sequencing and to Clare Isacke and Chris Jones for useful discussions. The results shown here are, in part, based upon data generated by the TCGA Research Network: http://cancergenome.nih.gov/. This study makes use of METABRIC data generated by the Molecular Taxonomy of Breast Cancer International Consortium, with funding provided by Cancer Research UK and the British Columbia Cancer Agency Branch. We acknowledge NHS funding to the ICR/Royal Marsden Hospital Biomedical Research Centre.

The costs of publication of this article were defrayed in part by the payment of page charges. This article must therefore be hereby marked *advertisement* in accordance with 18 U.S.C. Section 1734 solely to indicate this fact.

Received May 29, 2020; revised October 12, 2020; accepted November 25, 2020; published first January 28, 2021.

References

1. Cancer Genome Atlas Network. Comprehensive molecular portraits of human breast tumours. Nature 2012;490:61–70.
2. Ciriello G, Gatza ML, Beck AH, Wilkerson MD, Rhie SK, Pastore A, et al. Comprehensive molecular portraits of invasive lobular breast cancer. Cell 2015; 163:506–19.
3. Cancer Genome Atlas Research Network. Comprehensive genomic characterization of squamous cell lung cancers. Nature 2012;489:519–25.
4. Han K, Pierce SE, Li A, Spees K, Anderson GR, Seoane JA, et al. CRISPR screens in cancer spheroids identify 3D growth-specific vulnerabilities. Nature 2020;580: 136–41.
5. Morrison E, Wai P, Leonidou A, Bland P, Khalique S, Farnie G, et al. Utilizing functional genomics screening to identify potentially novel drug targets in cancer cell spheroid cultures. J Vis Exp 2016:54738. DOI: 10.3791/54738.
6. Ashworth A, Lord CJ. Synthetic lethal therapies for cancer: what's next after PARP inhibitors? Nat Rev Clin Oncol 2018;15:564–76.
7. Lord CJ, Tutt AN, Ashworth A. Synthetic lethality and cancer therapy: lessons learned from the development of PARP inhibitors. Annu Rev Med 2015;66: 455–70.
8. Masuda H, Baggerly KA, Wang Y, Zhang Y, Gonzalez-Angulo AM, Meric-Bernstam F, et al. Differential response to neoadjuvant chemotherapy among 7 triple-negative breast cancer molecular subtypes. Clin Cancer Res 2013; 19:5533–40.
9. Symmans WF, Wei C, Gould R, Yu X, Zhang Y, Liu M, et al. Long-term prognostic risk after neoadjuvant chemotherapy associated with residual cancer burden and breast cancer subtype. J Clin Oncol 2017;35:1049–60.
10. Collins FS, Varmus H. A new initiative on precision medicine. N Engl J Med 2015;372:793–5.
11. Maguire SL, Peck B, Wai PT, Campbell J, Barker H, Gulati A, et al. Three-dimensional modelling identifies novel genetic dependencies associated with breast cancer progression in the isogenic MCF10 model. J Pathol 2016; 240:315–28.
12. Banerji S, Cibulskis K, Rangel-Escareno C, Brown KK, Carter SL, Frederick AM, et al. Sequence analysis of mutations and translocations across breast cancer subtypes. Nature 2012;486:405–9.
13. Ding L, Ellis MJ, Li S, Larson DE, Chen K, Wallis JW, et al. Genome remodelling in a basal-like breast cancer metastasis and xenograft. Nature 2010;464: 999–1005.
14. Shah SP, Morin RD, Khattra J, Prentice L, Pugh T, Burleigh A, et al. Mutational evolution in a lobular breast tumour profiled at single nucleotide resolution. Nature 2009;461:809–13.

15. Shah SP, Roth A, Goya R, Oloumi A, Ha G, Zhao Y, et al. The clonal and mutational evolution spectrum of primary triple-negative breast cancers. Nature 2012;486:395–9.
16. Stephens PJ, Tarpey PS, Davies H, Van Loo P, Greenman C, Wedge DC, et al. The landscape of cancer genes and mutational processes in breast cancer. Nature 2012;486:400–4.
17. Wiederschain D, Wee S, Chen L, Loo A, Yang G, Huang A, et al. Single-vector inducible lentiviral RNAi system for oncology target validation. Cell Cycle 2009; 8:498–504.
18. Hornbeck PV, Zhang B, Murray B, Kornhauser JM, Latham V, Skrzypek E. PhosphoSitePlus, 2014: mutations, PTMs and recalibrations. Nucleic Acids Res 2015;43:D512–20.
19. He Z, Yang C, Guo G, Li N, Yu W. Motif-All: discovering all phosphorylation motifs. BMC Bioinformatics 2011;12:S22.
20. Anders L, Ke N, Hydbring P, Choi YJ, Widlund HR, Chick JM, et al. A systematic screen for CDK4/6 substrates links FOXM1 phosphorylation to senescence suppression in cancer cells. Cancer Cell 2011;20:620–34.
21. Kitagawa M, Higashi H, Jung HK, Suzuki-Takahashi I, Ikeda M, Tamai K, et al. The consensus motif for phosphorylation by cyclin D1-Cdk4 is different from that for phosphorylation by cyclin A/E-Cdk2. EMBO J 1996;15:7060–9.
22. Qiu X, Mao Q, Tang Y, Wang L, Chawla R, Pliner HA, et al. Reversed graph embedding resolves complex single-cell trajectories. Nat Methods 2017;14:979–82.
23. Anders S, Huber W. Differential expression analysis for sequence count data. Genome Biol 2010;11:R106.
24. Hinohara K, Wu HJ, Vigneau S, McDonald TO, Igarashi KJ, Yamamoto KN, et al. KDM5 histone demethylase activity links cellular transcriptomic heterogeneity to therapeutic resistance. Cancer Cell 2018;34:939–53.
25. Waggott D, Chu K, Yin S, Wouters BG, Liu FF, Boutros PC. NanoStringNorm: an extensible R package for the pre-processing of NanoString mRNA and miRNA data. Bioinformatics 2012;28:1546–8.
26. Li S, Shen D, Shao J, Crowder R, Liu W, Prat A, et al. Endocrine-therapy-resistant ESR1 variants revealed by genomic characterization of breast-cancer-derived xenografts. Cell Rep 2013;4:1116–30.
27. Gao J, Aksoy BA, Dogrusoz U, Dresdner G, Gross B, Sumer SO, et al. Integrative analysis of complex cancer genomics and clinical profiles using the cBioPortal. Sci Signal 2013;6:pl1.
28. Cerami E, Gao J, Dogrusoz U, Gross BE, Sumer SO, Aksoy BA, et al. The cBio cancer genomics portal: an open platform for exploring multidimensional cancer genomics data. Cancer Discov 2012;2:401–4.
29. Kamburov A, Wierling C, Lehrach H, Herwig R. ConsensusPathDB–a database for integrating human functional interaction networks. Nucleic Acids Res 2009; 37:D623–8.
30. Garcia-Alonso L, Iorio F, Matchan A, Fonseca N, Jaaks P, Peat G, et al. Transcription factor activities enhance markers of drug sensitivity in cancer. Cancer Res 2018;78:769–80.
31. Schug ZT, Peck B, Jones DT, Zhang Q, Grosskurth S, Alam IS, et al. Acetyl-CoA synthetase 2 promotes acetate utilization and maintains cancer cell growth under metabolic stress. Cancer Cell 2015;27:57–71.
32. Peck B, Schug ZT, Zhang Q, Dankworth B, Jones DT, Smethurst E, et al. Inhibition of fatty acid desaturation is detrimental to cancer cell survival in metabolically compromised environments. Cancer Metab 2016;4:6.
33. Razavi P, Chang MT, Xu G, Bandlamudi C, Ross DS, Vasan N, et al. The genomic landscape of endocrine-resistant advanced breast cancers. Cancer Cell 2018;34: 427–38.
34. Bannister AJ, Kouzarides T. The CBP co-activator is a histone acetyltransferase. Nature 1996;384:641–3.
35. Zhang J, Vlasevska S, Wells VA, Nataraj S, Holmes AB, Duval R, et al. The CREBBP acetyltransferase is a haploinsufficient tumor suppressor in B-cell lymphoma. Cancer Discov 2017;7:322–37.
36. Pasqualucci L, Dominguez-Sola D, Chiarenza A, Fabbri G, Grunn A, Trifonov V, et al. Inactivating mutations of acetyltransferase genes in B-cell lymphoma. Nature 2011;471:189–95.
37. Peifer M, Fernandez-Cuesta L, Sos ML, George J, Seidel D, Kasper LH, et al. Integrative genome analyses identify key somatic driver mutations of small-cell lung cancer. Nat Genet 2012;44:1104–10.
38. Mullighan CG, Zhang J, Kasper LH, Lerach S, Payne-Turner D, Phillips LA, et al. CREBBP mutations in relapsed acute lymphoblastic leukaemia. Nature 2011; 471:235–9.
39. Buffa FM, Harris AL, West CM, Miller CJ. Large meta-analysis of multiple cancers reveals a common, compact and highly prognostic hypoxia metagene. Br J Cancer 2010;102:428–35.
40. Sonveaux P, Vegran F, Schroeder T, Wergin MC, Verrax J, Rabbani ZN, et al. Targeting lactate-fueled respiration selectively kills hypoxic tumor cells in mice. J Clin Invest 2008;118:3930–42.
41. Curtis C, Shah SP, Chin SF, Turashvili G, Rueda OM, Dunning MJ, et al. The genomic and transcriptomic architecture of 2,000 breast tumours reveals novel subgroups. Nature 2012;486:346–52.
42. McGranahan N, Swanton C. Clonal heterogeneity and tumor evolution: past, present, and the future. Cell 2017;168:613–28.
43. Sanders DA, Ross-Innes CS, Beraldi D, Carroll JS, Balasubramanian S. Genome-wide mapping of FOXM1 binding reveals co-binding with estrogen receptor alpha in breast cancer cells. Genome Biol 2013;14:R6.
44. Barretina J, Caponigro G, Stransky N, Venkatesan K, Margolin AA, Kim S, et al. The Cancer Cell Line Encyclopedia enables predictive modelling of anticancer drug sensitivity. Nature 2012;483:603–7.
45. Chakraborty AA, Laukka T, Myllykoski M, Ringel AE, Booker MA, Tolstorukov MY, et al. Histone demethylase KDM6A directly senses oxygen to control chromatin and cell fate. Science 2019;363:1217–22.
46. Bhandari V, Li CH, Bristow RG, Boutros PC, Consortium P. Divergent mutational processes distinguish hypoxic and normoxic tumours. Nat Commun 2020; 11:737.
47. Jia D, Augert A, Kim DW, Eastwood E, Wu N, Ibrahim AH, et al. CREBBP loss drives small cell lung cancer and increases sensitivity to HDAC inhibition. Cancer Discov 2018;8:1422–37.
48. Lasko LM, Jakob CG, Edalji RP, Qiu W, Montgomery D, Digiammarino EL, et al. Discovery of a selective catalytic p300/CBP inhibitor that targets lineage-specific tumours. Nature 2017;550:128–32.
49. Ogiwara H, Sasaki M, Mitachi T, Oike T, Higuchi S, Tominaga Y, et al. Targeting p300 addiction in CBP-deficient cancers causes synthetic lethality by apoptotic cell death due to abrogation of MYC expression. Cancer Discov 2016;6:430–45.
50. Lv C, Zhao G, Sun X, Wang P, Xie N, Luo J, et al. Acetylation of FOXM1 is essential for its transactivation and tumor growth stimulation. Oncotarget 2016; 7:60366–82.
51. Rubio C, Martinez-Fernandez M, Segovia C, Lodewijk I, Suarez-Cabrera C, Segrelles C, et al. CDK4/6 inhibitor as a novel therapeutic approach for advanced bladder cancer independently of RB1 status. Clin Cancer Res 2019; 25:390–402.
52. Sayles LC, Breese MR, Koehne AL, Leung SG, Lee AG, Liu HY, et al. Genome-informed targeted therapy for osteosarcoma. Cancer Discov 2019; 9:46–63.
53. Edelman MJ, Redman MW, Albain KS, McGary EC, Rafique NM, Petro D, et al. SWOG S1400C (NCT02154490)-a phase II study of palbociclib for previously treated cell cycle gene alteration-positive patients with stage IV squamous cell lung cancer (Lung-MAP Substudy). J Thorac Oncol 2019;14:1853–9.
54. Teo ZL, Versaci S, Dushyanthen S, Caramia F, Savas P, Mintoff CP, et al. Combined CDK4/6 and PI3Kalpha inhibition is synergistic and immunogenic in triple-negative breast cancer. Cancer Res 2017;77:6340–52.
55. Schaer DA, Beckmann RP, Dempsey JA, Huber L, Forest A, Amaladas N, et al. The CDK4/6 inhibitor abemaciclib induces a T cell inflamed tumor microenvironment and enhances the efficacy of PD-L1 checkpoint blockade. Cell Rep 2018;22:2978–94.
56. Hassan Venkatesh G, Bravo P, Shaaban Moustafa Elsayed W, Amirtharaj F, Wojtas B, Abou Khouzam R, et al. Hypoxia increases mutational load of breast cancer cells through frameshift mutations. Oncoimmunology 2020;9:1750750.

Published OnlineFirst January 28, 2021; DOI: 10.1158/0008-5472.CAN-20-1822

Cancer Research
The Journal of Cancer Research (1916–1930) | The American Journal of Cancer (1931–1940)

AACR American Association for Cancer Research

3D Functional Genomics Screens Identify CREBBP as a Targetable Driver in Aggressive Triple-Negative Breast Cancer

Barrie Peck, Philip Bland, Ioanna Mavrommati, et al.

Cancer Res 2021;81:847-859. Published OnlineFirst January 28, 2021.